Measuring residual stresses in individual on-chip interconnects using synchrotron nanodiffraction

Zhang, Yaqian; Du, Leiming; Bäcke, Olof; Kalbfleisch, Sebastian; Zhang, Guoqi; Vollebregt, Sten; Hörnqvist Colliander, Magnus

DOI
10.1063/5.0192672

Publication date
2024

Document Version
Final published version

Published in
Applied Physics Letters

Applied Physics Letters

RESEARCH ARTICLE | FEBRUARY 21 2024

Measuring residual stresses in individual on-chip interconnects using synchrotron nanodiffraction

Yaqian Zhang ; Leiming Du ; Olof Bäcke ; Sebastian Kalbfleisch ; Guoqi Zhang ; Sten Vollebregt ; Magnus Hörnqvist Colliander

Appl. Phys. Lett. 124, 083501 (2024)
https://doi.org/10.1063/5.0192672

AIP Publishing

Measuring residual stresses in individual on-chip interconnects using synchrotron nanodiffraction

Cite as: Appl. Phys. Lett. **124**, 083501 (2024); doi: 10.1063/5.0192672
Submitted: 20 December 2023 · Accepted: 2 February 2024 ·
Published Online: 21 February 2024

Yaqian Zhang,[1] Leiming Du,[1] Olof Bäcke,[2] Sebastian Kalbfleisch,[3] Guoqi Zhang,[1] Sten Vollebregt,[1] and Magnus Hörnqvist Colliander[2,a)]

AFFILIATIONS

[1]Department of Microelectronics, Delft University of Technology, 2628 CD Delft, The Netherland
[2]Department of Physics, Chalmers University of Technology, Gothenburg, Sweden
[3]MAX IV Laboratory, Lund, Sweden

[a)]Author to whom correspondence should be addressed: magnus.colliander@chalmers.se

ABSTRACT

As the dimensions of interconnects in integrated circuits continue to shrink, an urgent need arises to understand the physical mechanism associated with electromigration. Using x-ray nanodiffraction, we analyzed the stresses in Blech-structured pure Cu lines subjected to different electromigration conditions. The results suggest that the measured residual stresses in the early stages of electromigration are related to relaxation of stresses caused by thermal expansion mismatch, while a developing current-induced stress leads to reductions in the residual stress after longer test times. These findings not only validate the feasibility of measuring stress in copper lines using nanodiffraction but also highlight the need for a further understanding, particularly through *in situ* electromigration experiments with x-ray nanodiffraction analysis.

The miniaturization of electronic devices is one of the most important driving forces for advances in the semiconductor industry. This trend has led on-chip interconnect to evolve from μm scale to nm scale in both width and height. As the interconnect dimensions are reduced, these narrow metal interconnects are also subjected to higher current densities.[1] The effects of electromigration (EM) have become more pronounced, making EM design a critical focus in the semiconductor field.[2–5]

Over the years, several multi-physics electromigration models have been developed to understand the failure mechanisms and predict the failure time.[6–13] However, there are errors in these models, and some have not yet been experimentally verified. Recognizing this gap, a new 3D general coupling model was proposed.[14] To support the theoretical framework and ensure its validity, experimental verification is essential. Moreover, a critical part of this verification process involves understanding the stress distribution within interconnects since stress migration affects EM differently under different conditions.[15]

X-ray nanodiffraction is a nondestructive method that offers high resolution for stress measurements in micro-sized structures, providing information about the lattice expansion along the entire interconnect. Several studies have characterized the stress distribution in interconnect structures. Lee *et al.* applied synchrotron x-ray techniques to study Sn electromigration and whisker growth in Blech structures. Their study not only indicated the Sn depletion at the cathode and whisker formation at the anode but also linked the observed Sn whiskering to internal stress resulting from atomic accumulation.[16]

In addition to Sn, copper (Cu), the main material in on-chip interconnects, has also been studied. Hsu *et al.* employed x-ray nanodiffraction to analyze thermal strain in nano-twinned Cu and regular Cu redistribution lines.[17] Lin *et al.* measured the strain at different points along a pure Cu line during electromigration and found non-uniform lattice expansion caused by electron flow and described the mechanism that leads to electromigration-induced failure, especially when the electron-induced strain exceeds the yield point.[18] However, the structure used in this paper is the dog-bone shape (mainly used to study the Joule heating effect during electromigration), with a metal line connected to sizable pads, which influenced the results through mechanical constraints.

In our research, we employed x-ray nanodiffraction to analyze pure copper with the Blech structure. This structure can be used not only to determine the critical length but also to measure the drifty velocity.[19] Notably, no existing studies have reported on the use of Blech structures in copper to examine potential residual stresses.

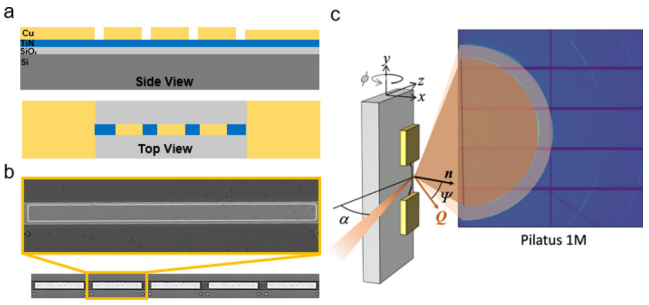

FIG. 1. (a) Schematic diagrams of the test samples. (b) Measured regions. (c) Schematic description of x-ray nanodiffraction setup and test samples.

The purpose of our study is to demonstrate that the residual stress in micro-sized Cu lines can be reliably measured using synchrotron nanodiffraction and that this method can measure the stress state under different EM test conditions. It can be considered as a proof-of-principle study, and we discuss the implications of the current *ex situ* results on possible strategies for future *in situ* measurements.

The sample fabrication process starts with the growth of 300 nm thick silicon dioxide (SiO_2) by thermal oxidation on the silicon (100) substrate. Then, we deposited a 300 nm TiN film via sputtering, patterned it using lithography and etching, and conducted plasma etching to prevent oxide layer formation. Cu films with a thickness of 200 or 500 nm thick were sputtered onto the TiN layer at room temperature. The Blech structure is patterned by photolithography and wet etching, as shown in Fig. 1(a). The detailed process can be found elsewhere in our previous study.[20] As depicted in Fig. 1(b), the x-ray analysis focused on regions where the Cu stripes were 60 μm long and 4 μm wide, with each sample containing five sets of these stripes connected in series.

The electromigration tests were conducted using an in-house setup, with the equipment specifics available in a previous work.[20] Samples were tested in a 3.75×10^{-6} Torr vacuum to avoid oxidation and under different current stresses and temperatures. The testing details for each sample are provided in Table I. After the test, the microstructures of each sample under different conditions were examined using scanning electron microscopy (SEM, Hitachi Regulus 8230).

The nanodiffraction measurements were performed using the nanodiffraction endstation[21] at the NanoMAX beamline[22] at MAX IV Laboratory in Lund, Sweden. At this beamline, a spatial resolution down to 50 nm can be reached, allowing studies of very small samples. It accommodates two optical microscopes used to navigate to the measurement position and align the sample to the x-ray focal position. Throughout the measurement process, a monochromatic x-ray beam with an energy of 14 keV and a spot size of 62 nm in the focal plane of the Kirkpatrick–Baez (KB) mirror focusing optics was employed.[23] The diced samples were vertically mounted on aluminum flat holders, as shown in Fig. 1(c), and the diffracted signal was collected in reflection geometry by a downstream Pilatus 1M area detector at a sample-to-detector distance of 148.1 mm (a LaB6 standard calibrated the position).

The Cu lines of interest were located within 50 μm from the downstream edge of the Si wafer. Coarse positioning was performed by tilting the samples up to 30° around the ω axis, which allowed visual access for the online optical microscope. Once the line was correctly positioned, the sample was tilted back to give an incidence angle $\alpha = 2°$, in order to prevent obstruction of the convergent beam by upstream structures on the chip and to minimize the shadowing of the detector by the downstream part of the substrate. The geometry allowed us to capture half of the Debye–Scherrer rings corresponding to (111) and (200) peaks of Cu.

Each line was scanned using the x–y piezo stage on top of the ω rotation stage, and the total intensity in each detector image allowed the identification of patterns originating from the Cu line (which provides a significantly stronger signal than TiN, etc.), see Fig. 2(a). Figure 2(b) shows the sum of all diffraction patterns obtained from the 500 nm thick as-fabricated sample, indicating the diffraction rings and the definition of the azimuthal angle χ. Figure 2(c) shows a caked 2D integration (10° cakes) of the summed detector image, centered around the (200) peak. It must be mentioned that the gaps in the detector and the presence of the beam stop (which were masked during the reduction with PyFAI v2023.1[24]) significantly affect the region $-20 \leq \chi \leq 20°$ [see gray rectangle in Fig. 2(d) where a smaller cake angle more clearly reveals the gaps in the data]. The peak position (d-spacing) of the (200) reflection (d_{200}) was extracted from each cake by the fitting of a pseudo-Voigt shape function using the *Lmfit* package[25] in Python, and it can be seen that the fits in the region $-20 \leq \chi \leq 20°$ are strongly affected [Fig. 2(e)]. This region is, therefore, excluded from the analysis. To find the residual stress, σ, we use the $\sin^2\Psi$ method,

$$\frac{\partial d_{200}}{\partial \sin^2\Psi} = \frac{1}{2} S_2^{200} d_0 \sigma, \tag{1}$$

TABLE I. Residual stresses in the individual Cu lines for the tested samples, and the average stress where more than one line was measured. The errors reported for the individual lines are of the parameter standard errors from the linear fit of Eq. (1), while the errors reported for the average stresses are the standard deviation of the mean stress for all lines. In the table, h refers to the line thickness, J_{EM} to the applied current density, and T_{EM} and t_{EM} to the time and temperature, respectively, for electromigration testing.

h (nm)	J_{EM} (MA cm^{-2})	T_{EM} (°C)	t_{EM} (h)	Residual stress, σ (MPa)			
				Line 1	Line 2	Line 3	Average
500	...	...	...	175 ± 18	...	...	...
200	...	...	...	145 ± 19	118 ± 19	127 ± 15	130 ± 14
500	1.7	250	5	337 ± 41	365 ± 54	386 ± 29	363 ± 25
500	1.7	250	10	234 ± 35	322 ± 56	309 ± 34	288 ± 48
500	1.7	200	10	280 ± 28	262 ± 42	228 ± 36	257 ± 26
500	1.6	250	10	350 ± 40	260 ± 38	274 ± 32	295 ± 48

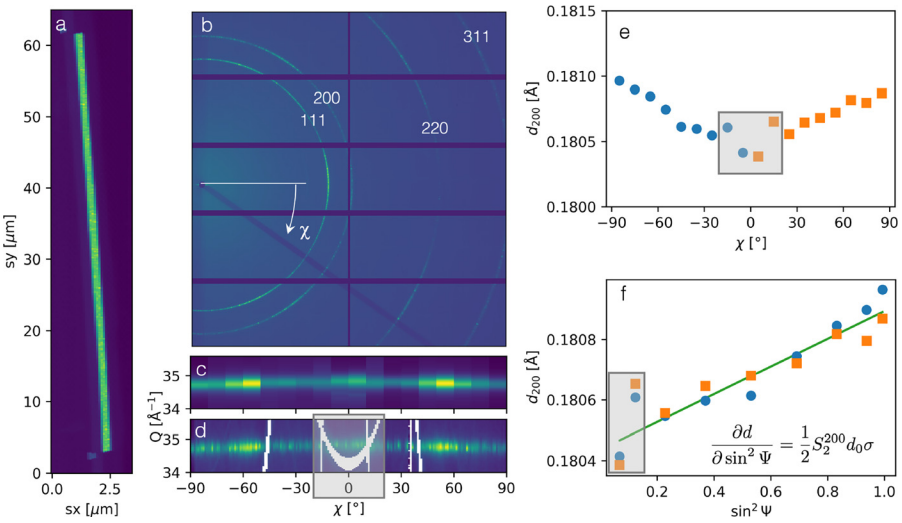

FIG. 2. (a) Total intensity patterns from the Cu line. (b) Summed diffraction patterns from 500 nm thick as-fabricated sample. (c) A caked 2D integration of the summed detector image. (d) Impact of detector gaps and beam stop on the diffraction pattern. (e) Fitted peak position of the (200) reflection. (f) Linear fitting of d_{200} vs $\sin^2\Psi$.

where $\Psi = \arccos[\cos(\chi)\cos(2\theta)]$ is the angle between the diffraction vector Q and the surface normal [see Fig. 1(d)], $1/2S^{200}$ is the diffraction elastic constant for Cu (here calculated using single crystal elastic constants[26] and the isotropic Kröner approximation in the IsoDEC software[27]), and d_0 is the y-axis intercept of a linear fit of d_{200} vs $\sin^2\Psi$. Notably, this method assumed an equi-biaxial stress state, which is confirmed by the very small difference between data from positive and negative χ [Fig. 2(f)]. There is a tendency for non-linearity of d_{200} vs $\sin^2\Psi$, which is likely due to the (111) texture of the Cu line, seen from the varying intensity distribution of the diffraction peaks along χ (Fig. S1 in the supplementary material). This affected the (111) peak to a much larger extent, giving pronounced non-linearity (although still no systematic differences between positive and negative χ, confirming the absence of shear stresses). For this reason, the (200) reflection was used for stress evaluation in the present case. We also note that the value of $1/2S_2^{200}$ was calculated for a sample with random texture, but as the non-linearity of the d_{200} vs $\sin^2\Psi$ curve is limited, the effect should not be profound.

For the as-fabricated 500 nm sample, the resulting average value of the residual stress in the entire Cu line is $\sigma = 175 \pm 18$ MPa (only a single line was measured, and the error is the standard error of the linear fit). The 200 nm sample had lower stress, $\sigma = 130 \pm 14$ MPa (average and standard deviation of three lines, see Table I for the values and errors of individual lines).

The residual stresses in the untested samples are presumably due to a mismatch of the coefficients of thermal expansion (CTE) between Cu and the substrate and originate from the fact that during the lithography process of Cu film, the wafer is placed on the heating platform at 115 °C to bake the photoresist on the surface. Ignoring the effect of the intermediate SiO_2 and TiN layer, for simplicity, the temperature corresponding to the measured stress levels can be estimated from the following relationship:

$$\sigma = E_{Cu}(\alpha_{Cu} - \alpha_{Si})\Delta T, \tag{2}$$

where $E_{Cu} = 130$ GPa is the elastic modulus of Cu, $\alpha_{Cu} = 16.6 \times 10^{-6}\,K^{-1}$ and $\alpha_{Si} = 4 \times 10^{-6}\,K^{-1}$ are the coefficients of thermal expansion (CTEs) of Cu and Si, respectively, and ΔT is the temperature difference. The measured stresses for the as-deposited states agree well with the sample temperature during the Cu litho process being around 115 °C (which corresponds to 155 MPa). The difference between the two samples (500 and 200 nm) indicates that there may be an additional thickness effect, which is frequently observed in thin-film systems, including Cu film.[28] However, the difference is only statistically significant at a confidence level of 11% (as estimated from a two-sample t-test), and due to the limited statistics from the single line measured for the 500 nm sample, we are not able to confirm this difference. Additional tests, with better statistics and several film thicknesses, should be performed to investigate the existence and extent of a thickness effect.

The effects of EM were explored by measuring a range of samples exposed to varying combinations of current, temperature, and loading time. The quality of the diffraction patterns (statistics) became worse after EM testing, and a slightly coarser caking scheme (14 cakes, corresponding to a cake angle of 12.9°) was used to improve the statistics in each individual cake. Summed detector images, caked data, and final d_{200} vs $\sin^2\Psi$ fits are shown for all samples in the supplementary material (Figs. S2–S7). For each sample, three separate lines were selected for measurement.

Figure 3 shows the results for all investigated conditions. After 5 h at 250 °C with $J_{EM} = 1.7$ MA cm^{-2}, the stress increased to 362 ± 25 MPa, but after 10 h, it dropped to 288 ± 48 MPa. It should be noted, however, that the difference is only statistically significant at a confidence level of 8%, as estimated from a two-sample t-test, suggesting further research is needed for confirmation. SEM images in Fig. 4(a) show EM tested at $J_{EM} = 1.7$ MA cm^{-2} and 250 °C. At the cathode side, small defects can be observed on the surface after 5 h of EM testing. With the testing time extended to 10 h, the void size increases. The increased formation of hillocks can be seen at the anode with increasing testing time.

To further investigate the impact of EM conditions on residual stress, we performed comparative measurements, including different current densities and temperatures. EM analysis, as depicted in Fig. 4(b), shows after 10 h with temperature reduced to 200 °C that hillock formation was significantly less. Additionally, there were no voids or surface defects on the cathode side. This situation is similar to

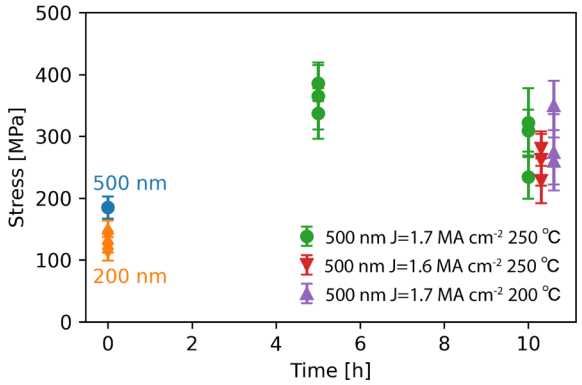

FIG. 3. Measured residual stress after different EM conditions.

that observed when the current density is reduced to 1.6 MA cm^{-2}. The measured residual stresses, however, did not change significantly as a result of lowering the current density or reducing the testing temperature. The stresses after 10 h at both 1.7 MA cm^{-2} and 200 °C (295 ± 45 MPa), and 1.6 MA cm^{-2} at 250 °C 257 ± 26 MPa, were within the standard deviation span of the value after 10 h at 1.7 MA cm^{-2} and 250 °C reported above (288 ± 48 MPa).

We also tested samples at higher currents and with extended EM duration. When the current density reached $J_{EM} = 1.8$ MA cm^{-2} after 5 h at 250 °C, void size increased, and large hillocks were formed at the anode side, as shown in Fig. 4(c). It also led to changes in the microstructure, such as grain enlargement, which prevented reliable stress measurements. Similarly, as the testing time extended to 20 h, the voids and hillock regions grew larger, resulting in an undesirably large grain size under the current density of 1.7 MA cm^{-2} at 250 °C.

In examining the 500 nm samples tested at 1.7 MA cm^{-2} at 250 °C, an unexpected decreasing trend in residual stress between 5 and 10 h EM testing emerges. Initially, there is an increase in stress after 5 h compared to the as-deposited state, attributable to stress relaxation during the test. It is known that thin Cu films relax at temperatures exceeding roughly 200 °C,[29,30] and thus, the compressive stress developed during heating to 250 °C [−275 MPa for a room temperature stress of 175 MPa, according to Eq. (2)] should continuously relax toward zero during the test duration. Cooling will introduce thermal stresses in the tensile direction, and as the compressive stress has relaxed, the addition of the thermal stress will result in a higher tensile stress compared to the untested state. However, for un-capped Cu films, the relaxation process is generally not completed within 10 h in the temperature range of the present study.[31,32] Consequently, the sample tested at 10 h is expected to have even lower compressive stresses (more progressed relaxation) and exhibits even higher tensile stresses after cooling (here we note that the residual stress development during cooling is not linear with temperature due to relaxation processes,[29,30] but we assume that the behavior during cooling is similar after 5 and 10 h of testing). For the tensile stress to be lower after 10 h, the starting compressive stress during the cooling phase must be greater than that after 5 h, which contradicts the expected trend of advanced relaxation. This observed behavior strongly suggests that the current-induced stresses during the EM process (arising from volumetric strains due to the local changes in vacancy concentration produced by current-driven diffusion[14]) play a significant role. Development of

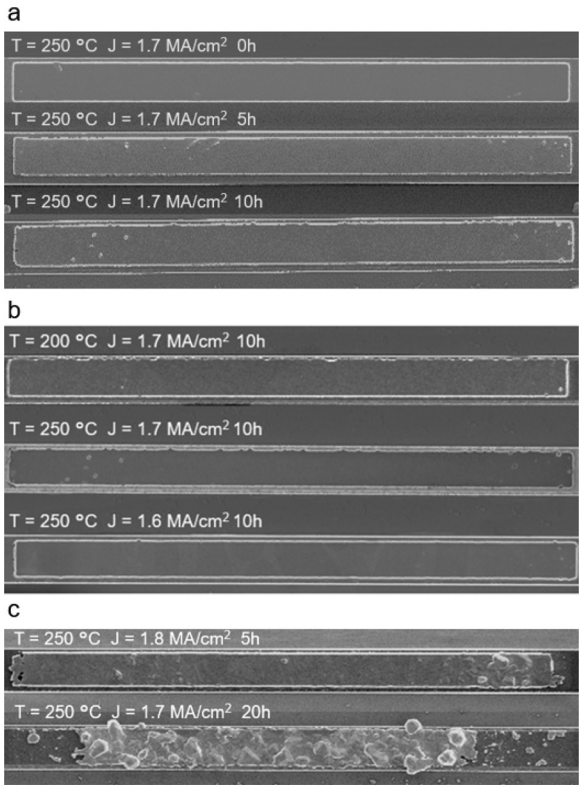

FIG. 4. SEM images of Blech structure lines after different EM conditions. (a) 60 μm stripes under $J_{EM} = 1.7$ MA cm^{-2} at 250 °C from 0 to 10 h; (b) 60 μm stripes under $J_{EM} = 1.7$ MA cm^{-2} and $J_{EM} = 1.6$ MA cm^{-2} at 200 and 250 °C at 10 h; and (c) 60 μm stripes under higher current density $J_{EM} = 1.8$ MA cm^{-2} at 5 h and extended EM duration $J_{EM} = 1.7$ MA cm^{-2} at 20 h.

an in-plane compressive stress component during EM has indeed been predicted from the general coupling model.[14] The coupled effects of elastic, thermal, and EM strain introduces a complex dynamic, where the fast relaxation dominates at shorter times, whereas the compressive stresses developed due to EM govern the behavior at longer times. We note that there may be further coupled effects in the presence of current stressing, such as generation of dislocations, the increased strain energy of which can accelerate recrystallization.

Furthermore, previous experimental studies and simulations[15,18] indicate that EM induces a stress gradient along the line, which can also be influenced by mechanical constraints.[18] We attempted spatially resolved analysis of the data from the 500 nm sample by dividing it into shorter segments and analyzing the parts individually, but as illustrated in the supplementary material (Fig. S8), this approach did not yield reliable results. To allow spatially resolved measurements, increased statistics are required, which could potentially be achieved by rocking the sample during measurements. Furthermore, using microbeams (in combination with sample rocking) will increase the time resolution and allow full-line (or even multi-line) mapping, thus supporting *in situ* measurements. The proposed approaches, however, remain to be explored.

In conclusion, our study revealed that it is possible to differentiate residual stress states in Cu lines in Blech structures obtained after EM testing under different conditions using x-ray nanodiffraction. The

results suggest that the measured residual stresses in the early stages of EM are related to relaxation of stresses caused by CTE mismatch, while the stress reduction observed after extended test duration results from interactions between the thermal mismatch stress and a developing current-induced compressive stress. *In situ* measurements are essential to verify this hypothesis and also permit investigations of current-induced, or current-enhanced, changes such as plastic deformation and recrystallization through peak width evolution and changes in the spottiness of the diffraction rings.

See the supplementary material for more details about the experiment results under different EM conditions.

This work was financially supported by the iRel40 project. iRel40 is a European co-founded innovation project that has been granted by the ECSEL Joint Undertaking (JU) under grant agreement No. 876659. The funding of the project comes from the Horizon 2020 research program and participating countries. We also acknowledge MAX IV Laboratory for time on Beamline [NanoMAX] under Proposal (No. 20221056). Research conducted at MAX IV, a Swedish national user facility, is supported by the Swedish Research council under Contract No. 2018-07152, the Swedish Governmental Agency for Innovation Systems under Contract No. 2018-04969, and Formas under Contract No. 2019-02496.

AUTHOR DECLARATIONS

Conflict of Interest

The authors have no conflicts to disclose.

Author Contributions

Yaqian Zhang and Leiming Du contributed equally to this work.

Yaqian Zhang: Formal analysis (equal); Investigation (equal); Methodology (equal); Visualization (equal); Writing – original draft (equal); Writing – review & editing (equal). **Leiming Du:** Conceptualization (equal); Investigation (equal); Methodology (equal); Writing – original draft (equal); Writing – review & editing (equal). **Olof Bäcke:** Investigation (equal). **Sebastian Kalbfleisch:** Investigation (supporting); Methodology (supporting); Writing – review & editing (supporting). **Guoqi Zhang:** Funding acquisition (equal); Supervision (equal). **Sten Vollebregt:** Supervision (equal); Writing – review & editing (equal). **Magnus Hörnqvist Colliander:** Conceptualization (equal); Data curation (equal); Formal analysis (equal); Investigation (equal); Methodology (equal); Visualization (equal); Writing – original draft (equal); Writing – review & editing (equal).

DATA AVAILABILITY

The data that support the findings of this study are available from the corresponding author upon reasonable request.

REFERENCES

[1]J. H. Lau, "Recent advances and trends in advanced packaging," IEEE Trans. Compon., Packag., Manuf. Technol. **12**, 228–252 (2022).
[2]P. S. Ho and T. Kwok, "Electromigration in metals," Rep. Prog. Phys. **52**, 301 (1989).
[3]K.-N. Tu, "Recent advances on electromigration in very-large-scale-integration of interconnects," J. Appl. Phys. **94**, 5451–5473 (2003).
[4]C. M. Tan and A. Roy, "Electromigration in ULSI interconnects," Mater. Sci. Eng., R **58**, 1–75 (2007).
[5]K.-N. Tu, Y. Liu, and M. Li, "Effect of Joule heating and current crowding on electromigration in mobile technology," Appl. Phys. Rev. **4**, 011101 (2017).
[6]M. Shatzkes and J. Lloyd, "A model for conductor failure considering diffusion concurrently with electromigration resulting in a current exponent of 2," J. Appl. Phys. **59**, 3890–3893 (1986).
[7]R. Kirchheim, "Stress and electromigration in Al-lines of integrated circuits," Acta Metall. Mater. **40**, 309–323 (1992).
[8]M. A. Korhonen, P. Bo/Rgesen, K.-N. Tu, and C.-Y. Li, "Stress evolution due to electromigration in confined metal lines," J. Appl. Phys. **73**, 3790–3799 (1993).
[9]J. Clement and C. Thompson, "Modeling electromigration-induced stress evolution in confined metal lines," J. Appl. Phys. **78**, 900–904 (1995).
[10]M. Sarychev, Y. V. Zhitnikov, L. Borucki, C.-L. Liu, and T. Makhviladze, "General model for mechanical stress evolution during electromigration," J. Appl. Phys. **86**, 3068–3075 (1999).
[11]V. Sukharev, E. Zschech, and W. D. Nix, "A model for electromigration-induced degradation mechanisms in dual-inlaid copper interconnects: Effect of microstructure," J. Appl. Phys. **102**, 053505 (2007).
[12]V. Sukharev and E. Zschech, "A model for electromigration-induced degradation mechanisms in dual-inlaid copper interconnects," in *IEEE International Integrated Reliability Workshop Final Report* (IEEE, 2004), pp. 79–85.
[13]A. M. Maniatty, J. Ni, Y. Liu, and H. Zhang, "Effect of microstructure on electromigration-induced stress," J. Appl. Mech. **83**, 011010 (2016).
[14]Z. Cui, X. Fan, and G. Zhang, "General coupling model for electromigration and one-dimensional numerical solutions," J. Appl. Phys. **125**, 105101 (2019).
[15]Z. Cui, X. Fan, Y. Zhang, S. Vollebregt, J. Fan, and G. Zhang, "Coupling model of electromigration and experimental verification—Part I: Effect of atomic concentration gradient," J. Mech. Phys. Solids **174**, 105257 (2023).
[16]P.-T. Lee, W.-Z. Hsieh, C.-Y. Lee, S.-C. Tseng, M.-T. Tang, C.-Y. Chiang, C. Kao, and C.-E. Ho, "Synchrotron x-ray study of electromigration, whisker growth, and residual strain evolution in a Sn Blech structure," Scr. Mater. **214**, 114682 (2022).
[17]W.-Y. Hsu, I.-H. Tseng, C.-Y. Chiang, K. Tu, and C. Chen, "Distribution of elastic stress as a function of temperature in a 2-μm redistribution line of Cu measured with x-ray nanodiffraction analysis," J. Mater. Res. Technol. **20**, 2799–2808 (2022).
[18]S.-K. Lin, Y.-c. Liu, S.-J. Chiu, Y.-T. Liu, and H.-Y. Lee, "The electromigration effect revisited: Non-uniform local tensile stress-driven diffusion," Sci. Rep. **7**, 3082 (2017).
[19]I. Blech, "Diffusional back flows during electromigration," Acta Mater. **46**, 3717–3723 (1998).
[20]Y. Zhang, J. Mo, Z. Cui, S. Vollebregt, and G. Zhang, "Electromigration-induced local dewetting in Cu films," in *IEEE International Interconnect Technology Conference (IITC) and IEEE Materials for Advanced Metallization Conference (MAM)(IITC/MAM)* (IEEE, 2023).
[21]D. Carbone, S. Kalbfleisch, U. Johansson, A. Björling, M. Kahnt, S. Sala, T. Stankevic, A. Rodriguez-Fernandez, B. Bring, Z. Matej, P. Bell, D. Erb, V. Hardion, C. Weninger, H. Al-Sallami, J. Lidon-Simon, S. Carlson, A. Jerrebo, B. Norsk Jensen, A. Bjermo, K. Åhnberg, and L. Roslund, "Design and performance of a dedicated coherent x-ray scanning diffraction instrument at beamline NanoMAX of MAX IV," J. Synchrotron Radiat. **29**, 876–887 (2022).
[22]U. Johansson, D. Carbone, S. Kalbfleisch, A. Björling, M. Kahnt, S. Sala, T. Stankevic, M. Liebi, A. Rodriguez Fernandez, B. Bring *et al.*, "NanoMAX: The hard x-ray nanoprobe beamline at the MAX IV Laboratory," J. Synchrotron Radiat. **28**, 1935–1947 (2021).
[23]A. Björling, S. Kalbfleisch, M. Kahnt, S. Sala, K. Parfeniukas, U. Vogt, D. Carbone, and U. Johansson, "Ptychographic characterization of a coherent nanofocused x-ray beam," Opt. Express **28**, 5069–5076 (2020).
[24]J. Kieffer, V. Valls, N. Blanc, and C. Hennig, "New tools for calibrating diffraction setups," J. Synchrotron Radiat. **27**, 558–566 (2020).
[25]M. Newville, T. Stensitzki, D. B. Allen, M. Rawlik, A. Ingargiola, and A. Nelson, "LMFIT: Non-linear least-square minimization and curve-fitting for Python," Astrophysics Source Code Library, 2016.
[26]H. M. Ledbetter and E. R. Naimon, "Elastic properties of metals and alloys. II. Copper," J. Phys. Chem. Ref. Data **3**, 897–935 (1974).
[27]T. Gnäupel-Herold, "ISODEC: Software for calculating diffraction elastic constants," J. Appl. Crystallogr. **45**, 573–574 (2012).
[28]J. Liu, B. Xu, H. Wang, X. Cui, L. Zhu, and G. Jin, "Effects of film thickness and icrostructures on residual stress," Surf. Eng. **32**, 178–184 (2016).

[29]R. P. Vinci, E. M. Zielinski, and J. C. Bravman, "Thermal strain and stress in copper thin films," Thin Solid Films **262**, 142–153 (1995).
[30]K. Tanaka and Y. Akiniwa, "In-situ measurements of internal stresses in copper thin films during thermal cycling using synchrotron x-rays," in *Micro-Nanomechatronics and Human Science, 2004 and the Fourth Symposium Micro-Nanomechatronics for Information-Based Society* (IEEE, 2004).
[31]N. Singh, A. F. Bower, D. Gan, S. Yoon, P. S. Ho, J. Leu, and S. Shankar, "Numerical simulations and experimental measurements of stress relaxation by interface diffusion in a patterned copper interconnect structure," J. Appl. Phys. **97**, 013539 (2005).
[32]D. Gan, P. S. Ho, R. Huang, J. Leu, J. Maiz, and T. Scherban, "Isothermal stress relaxation in electroplated Cu films. I. Mass transport measurements," J. Appl. Phys. **97**, 103531 (2005).